

## Article

# Electromagnetic Vibration Characteristics of High-Frequency Transformer under DC Bias with Different Winding Structures

Haibo Ding, Wenliang Zhao \*, Min Li, Li Zhang and Youliang Sun

School of Electrical Engineering, Shandong University, Jinan 250061, China; dinghb1998@163.com (H.D.); min\_li2022@163.com (M.L.); li\_zhang2022@163.com (L.Z.); sun\_youliang2022@163.com (Y.S.)

\* Correspondence: wlzhao@sdu.edu.cn; Tel.: +86-139-5313-5625

**Abstract:** The core excitation saturation and vibration caused by DC bias are one of the important considerations in the design of high-frequency transformer (HFT). This paper studies the electromagnetic vibration characteristics of DC biased HFT with different winding structures. The vibration mechanism of iron core and winding under DC bias is analyzed. The optimal topology size of HFT is determined by area product (AP) method. In addition, the electromagnetic vibration multi-physical coupling model of a 500 V HFT under DC bias is established. At the same time, the electromagnetic vibration characteristics of interleaved winding and continuous winding of HFT are compared. The research shows that the current fluctuation of interleaved winding is smaller than that of continuous winding because of its ability to withstand impulse voltage. In addition, the average loss and maximum vibration displacement of HFT with entanglement winding are reduced in different degrees. The above research rules have guiding significance for the design of HFT and the method of suppressing DC bias.

**Keywords:** high-frequency transformer; DC bias; vibration mechanism; multi-physics coupling model; interleaved winding; continuous winding



**Citation:** Ding, H.; Zhao, W.; Li, M.; Zhang, L.; Sun, Y. Electromagnetic Vibration Characteristics of High-Frequency Transformer under DC Bias with Different Winding Structures. *Processes* **2023**, *11*, 1185. <https://doi.org/10.3390/pr11041185>

Academic Editor: Wen-Jer Chang

Received: 7 March 2023

Revised: 2 April 2023

Accepted: 10 April 2023

Published: 12 April 2023



**Copyright:** © 2023 by the authors. Licensee MDPI, Basel, Switzerland. This article is an open access article distributed under the terms and conditions of the Creative Commons Attribution (CC BY) license (<https://creativecommons.org/licenses/by/4.0/>).

## 1. Introduction

High-frequency transformer (HFT) is an important part of transmission and distribution system, and its security and stability are critical to the stable operation of power grid [1]. With the continuous development of the power industry and high-voltage DC transmission technology, the current of DC transmission system under monopolar ground circuit operation flows through the neutral point of HFT, causing DC bias of transformer [2–4]. DC bias increases the noise and local overheating, which is extremely unfavorable to the safe operation of power grid [5,6]. Therefore, the DC bias phenomenon of HFT is widely concerned. It is necessary to analyze the winding vibration characteristics under different DC bias level.

DC bias is caused by the following factors: When DC transmission is operated in monopolar earth loop mode or bipolar unbalanced mode, DC current invades the AC system. The grounding transformer generates DC bias [7–9]. Furthermore, the geomagnetic storm causes the geomagnetically induced current, which produces DC bias in grounding transformer [10,11]. Therefore, DC bias becomes an urgent problem in power system. In order to reduce the influence of DC bias of transformers, it is important to choose the winding type and winding mode suitable for transformer reasonably to restrain DC bias. Because there are differences in capacity and voltage of transformer, the structure characteristics of winding are also different. Generally, the winding of transformer can be divided into two different forms, one is layer type and the other is pie. Among them, the inner shielded winding is inserted into capacitive winding, which has a wide application range. Spiral winding is mainly used for low-voltage winding of transformer due to its low voltage and large current. Continuous winding is simple and

easy to operate, but it has the low series capacitance and the poor voltage distribution effect under the impact voltage. The biggest difference between interleaved winding and continuous winding is that the inter-turn capacitance is larger, and the applicable voltage level is higher [12–14]. In addition, the research on the electromagnetic vibration characteristics of transformers under DC bias are studied widely. In [15], a single-phase transformer simulation model is established, and the influence of DC bias component on transformer excitation characteristics through harmonic analysis is studied. In [16], a two-dimensional model in which two mass elements are used to represent a winding is put forward, and the elements are connected by springs. However, this model can only consider the elastic characteristics of the pad when it is equivalent to a spring, and it fails to consider the material characteristics of the pad and the influence of winding geometry on vibration. This leads to an error with the actual winding vibration. The other solution is to use a finite element to model and analyze. In [17], the electromagnetic vibration characteristics of transformer under rated load by using finite element model are studied, and are verified by experiments. In [18], the short-circuit electromotive force in short circuit and the winding stress characteristics under the influence of electromotive force are calculated, and the stress distribution at different positions of winding is obtained. In [19], the vibration and noise spatial distribution of transformer core are studied, and the maximum value of vibration and noise appeared at the joint of the core is found. In [20], the influence of DC bias on the core magnetic density and magnetostrictive is studied by establishing a three-dimensional model of single-phase transformer. In [21], an experimental study on the transformer under the condition of DC bias is conducted, and DC bias would accelerate the saturation of transformer core. Besides, the noise would increase and tend to saturation with the increase of DC bias. However, when studying the electrodynamic force of the winding, the existing research is less about the vibration characteristics of the winding when a short-circuit fault occurs under DC bias. When the transformer is under the influence of magnetic bias for a long time, even if the magnetic bias current is not large, its mechanical stability is affected in the long run. Meanwhile, the probability of winding damage increases when a short circuit fault occurs. Above all, a large number of facts show that the current research on the suppression mechanism of transformer winding structure to DC bias and the electromagnetic vibration characteristics under DC bias is not perfect, and there are still some problems to be solved [22–24].

In this paper, a single-phase high-power HFT is designed to research electromagnetic vibration characteristics with interleaved winding and continuous winding. Based on the field circuit coupling finite element method (FEM), the multi-physics coupling models of electromagnetic and stress field are established. Furthermore, the electromagnetism and vibration characteristics of HFT based on interleaved winding and continuous winding under different DC bias levels are calculated and compared. The transformer vibration characteristics under different DC bias is analyzed, and the vibration law of interleaved winding and continuous winding under DC bias are studied.

## 2. Electromagnetic Vibration Mechanism of High-Frequency Transformer under DC Bias

### 2.1. Electromagnetic Field

The magnetic flux path of the single-phase transformer is shown in Figure 1. In the Figure,  $\Phi_1$  is the main magnetic flux of the transformer,  $\Phi_2$  is the leakage flux of the transformer primary winding,  $U_1$  and  $U_{20}$  are the primary winding applied voltage and secondary winding no-load voltage, respectively,  $e_1$  and  $e_2$  are the induced electromotive force (EMF) of the primary and secondary winding, respectively, and  $i_{10}$  is the no-load current.

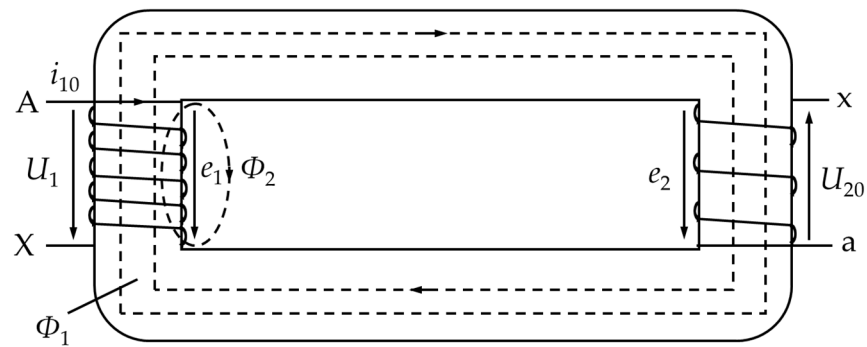


Figure 1. Single-phase HFT magnetic flux diagram.

According to Kirchhoff's voltage law, the voltage equations of the primary and secondary windings at no-load can be obtained:

$$\begin{cases} U_1 = i_{10}R_1 - e_1 = i_{10}R_1 + N_1 \frac{d\Phi}{dt} \\ U_{20} = e_2 = -N_2 \frac{d\Phi}{dt} \end{cases}, \quad (1)$$

where  $R_1$  is the primary winding resistance.  $N_1$  and  $N_2$  are the turns of the primary winding and secondary winding, respectively.  $\Phi$  is the interlinkage flux with the primary winding, and it is related to the frequency of the AC source.

Assuming that the average length of the magnetic circuit of the iron core is  $l$ , according to Ampere's law, the magnetomotive force balance equation under DC bias can be obtained as follows:

$$N_1(i_{10} + I_{DC}) = Hl = \frac{B}{\mu}l = \frac{\Phi}{\mu S}l, \quad (2)$$

where  $I_{DC}$  is the DC current applied to the primary winding, the DC bias magnetic flux generated is  $\Phi_0$ , and the total main magnetic flux of iron core is  $\Phi = \Phi_0 + \Phi_1$ .

The above electromotive force and magnetomotive force balance equations can be sorted out to obtain the magnetic circuit coupling equation as follows:

$$U_1 = R_1 i_{10} + \frac{N_1^2}{R_m} \frac{di_{10}}{dt}, \quad (3)$$

where  $R_m = \frac{l}{\mu S}$  is the magnetoresistance, which is nonlinear. The B–H curve of nanocrystalline material FT-3W is shown in Figure 2. The density of nanocrystalline material is  $7.25 \text{ g/cm}^3$ , the saturation magnetic density is  $1.18 \text{ T}$ , and the strip thickness is  $18 \text{ }\mu\text{m}$ .

## 2.2. Stress Field

Through the transient analysis of electromagnetic field above, the transient value of electromagnetic force on iron core and winding with time can be obtained. The strain of iron core and winding material can be transformed into excitation force by using the principle of elasticity. Considering that the silicon steel sheet of iron core is isotropic, the volume force density  $f_0$  of the iron core under magnetic field force is

$$f_0 = JB - \frac{1}{2}H^2 \nabla \mu' + \frac{1}{2} \nabla \left( H^2 \tau \frac{\partial \mu}{\partial \tau} \right), \quad (4)$$

where  $J$  is the current density.  $B$  is the magnetic induction intensity;  $H$  is the magnetic field intensity.  $\mu'$  is the medium permeability.  $\tau$  is the volume density of the medium. DC bias causes forced vibration of transformer windings. Since the electromagnetic force on the windings is proportional to the square of the current, the electromagnetic force  $F$  and displacement  $Z$  on the transformer windings are, respectively,

$$F_n(t) = b \left( A_0^2 + \frac{1}{2} I_m^2 \right) + 2bA_0 I_m \cos \omega t + \frac{1}{2} b I_m^2 \cos 2\omega t, \quad (5)$$

$$M \frac{d^2 z}{dt^2} + C \frac{dz}{dt} + Kz = F + Mg, \quad (6)$$

where  $A_0 = \int_{t_0}^{t_0+T} i(t) dt$ .  $T$  is the sinusoidal power supply cycle.  $b$  is the proportional coefficient of electromagnetic force and current.  $I_m$  is the amplitude of sinusoidal power supply.  $M$  is the coil mass.  $C$  is the vibration damping coefficient.  $K$  is the insulation stiffness coefficient.

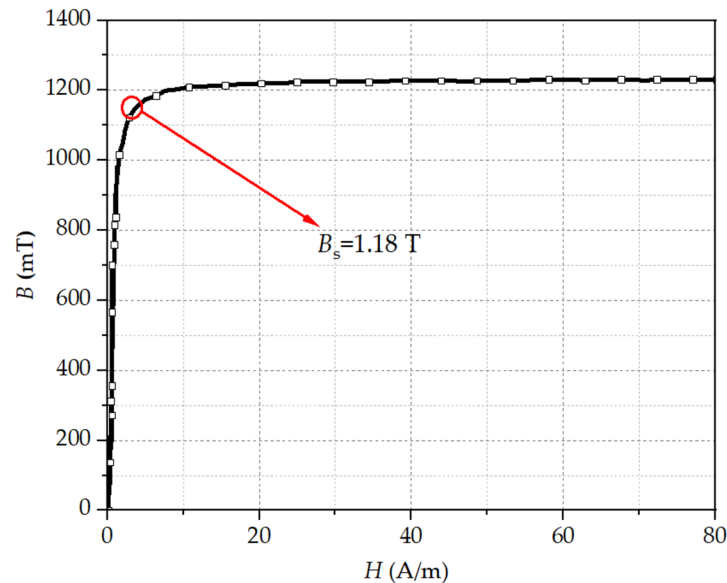


**Figure 2.** B–H curve of nanocrystalline material.

### 3. Modeling and DC Bias Design of High-Frequency Transformer

In order to analyze the physical and operating characteristics of HFT under DC bias, the model of single-phase 500 V HFT is established, and the corresponding DC bias external circuit is built. The HFT with continuous winding is shown in Figure 3a. For the purposes of suppressing the external impulse voltage, the HFT with interleaved winding is presented as shown in Figure 3b.

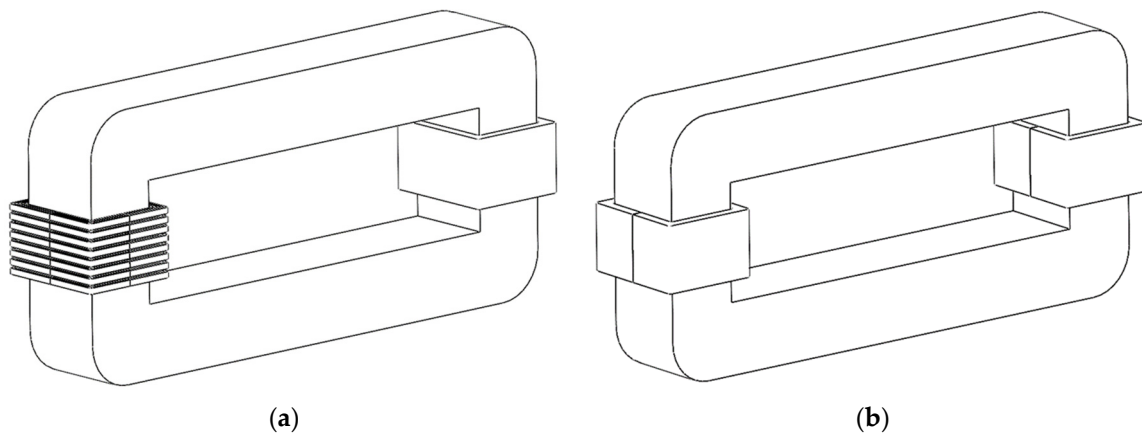


**Figure 3.** HFT model. (a) Interleaved windings; (b) Continuous windings.

### 3.1. Design of Winding

Due to the skin effect inside the wires, the inner conductive area is mainly concentrated on the surface. The effective cross-sectional area inside the wires is reduced, and the equivalent resistance is increased, which ultimately increases the winding loss. Therefore, it is very important to analyze the skin depth inside the windings, and the calculation method of the skin depth is as follows:

$$\delta = \frac{1}{\sqrt{\pi f \mu \sigma}} \quad (7)$$

where  $f$  ( $=10,000$  Hz) is the power supply frequency, and  $\mu$  ( $=4\pi \times 10^{-7}$  H/m) and  $\sigma$  ( $=6 \times 10^7$  S/m) are the permeability and conductivity of copper, respectively.

According to the calculation results, it can be determined that the skin depth is 0.65 mm. The skin effect caused by high-frequency current should be fully considered when the HFT windings are designed. Therefore, the winding diameter is generally set within two times of the skin depth. The conductor QZ-2 thick insulated polyester enameled flat copper wire can meet the requirements. Specific parameters are shown in Table 1.

**Table 1.** Wire Specific Parameters.

Item	Unit	Value
Model	/	QZ-2
Cross-sectional area	mm <sup>2</sup>	3.55
Resistivity	$\Omega \cdot m$	$1.67 \times 10^{-8}$
Length	mm	3.55
Width	mm	1.00

The winding method of the interleaved winding is basically the same as that of the continuous winding, except for the difference in the connection of turns. The interleaved winding is intertwined by the two adjacent sections of wire cakes in the continuous winding. In addition, the number of shunt wound wires is twice that of the parallel wires that constitute the turns. The continuous winding consists of several wire cakes made of paper-wrapped flat wires, and each wire cake is continuously wound by several turns in sequence. The winding model and its outspread diagram are shown in Figures 4 and 5, respectively. The inter-turn capacitance of interleaved winding cake is large, which compensates the capacitance-to-ground current. The interleaved winding is able to evenly distribute the impact voltage to each turn and wire cake under external impact such as DC bias, which is an advantage that the continuous winding does not have.

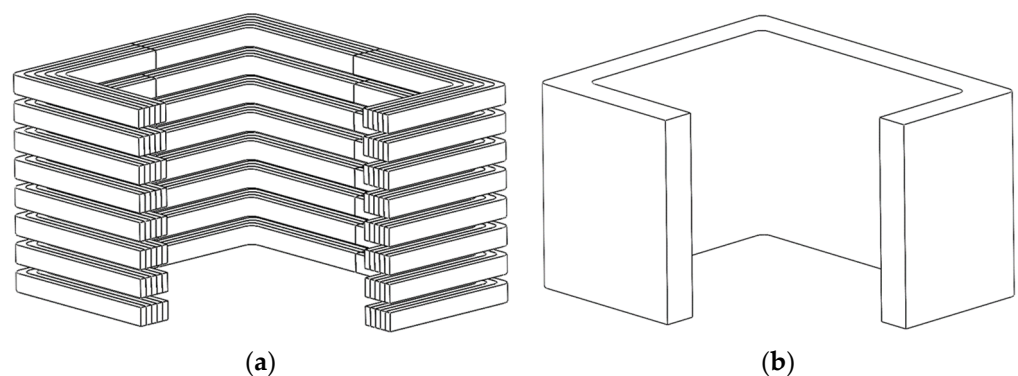


**Figure 4.** Grid side winding model. (a) Interleaved windings; (b) Continuous windings.

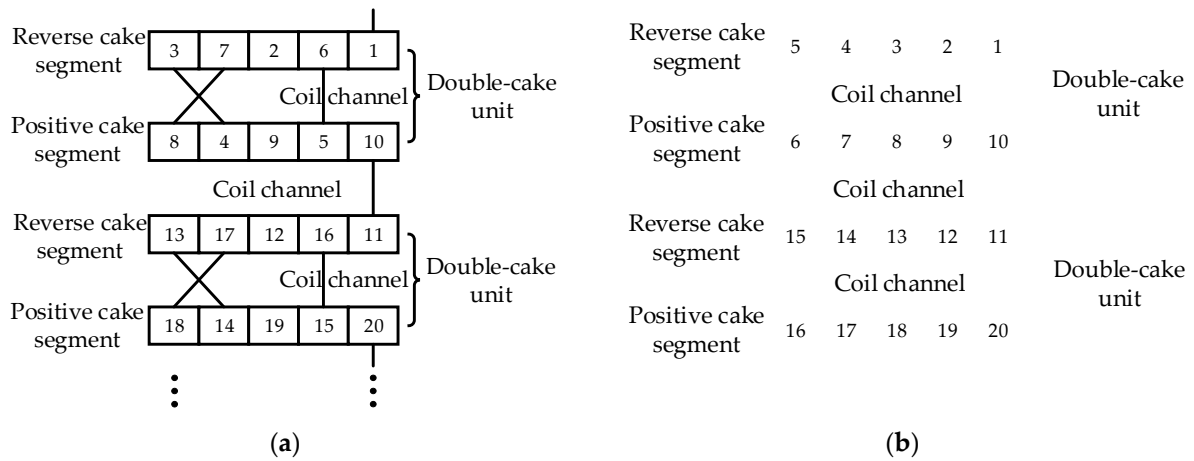


Figure 5. Outspread diagram of winding. (a) Interleaved windings; (b) Continuous windings.

3.2. HFT Model

Since C-type iron core has the advantages of small air gap, light weight, and high material utilization rate, C-type iron core structure is selected, which is made by docking two C-type structures. The specific structure diagram is shown in Figure 6.

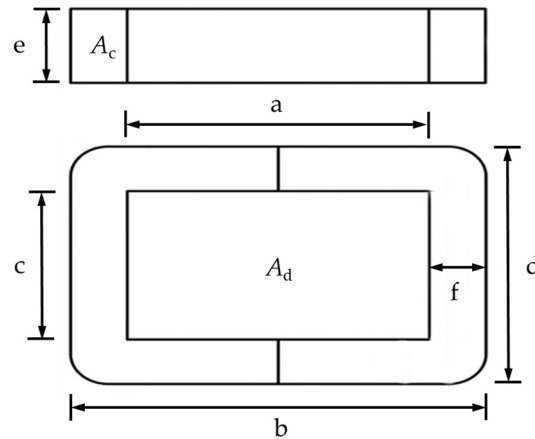


Figure 6. Schematic diagram of C-core, where, “a” and “c” are the length and height of iron core window, respectively. “b”, “e” and “d” are the length, width and height of core, respectively. “f” is the width of magnetic circuit. Ac is cross-sectional area of iron core. Ad is area of iron core window.

For HFT, the area product method ( $A_p$ ) is used to calculate the iron core parameters, as follows:

$$A_p = \left( \frac{S \times 10^4}{K_u f_w B_w K_d} \right)^{\frac{1}{1+x}}, \tag{8}$$

where  $S$  is the apparent power of HFT.  $K_u$  is the waveform coefficient.  $f_w$  is the operation frequency.  $B_w$  is the operation magnetic flux density.  $K_d$  is the iron core window coefficient.  $x$  is a constant related to the iron core. By substituting the correlation coefficient,  $A_p$  (Fe-based nanocrystalline) is  $262.4 \text{ cm}^4$ . The specific parameters of C-core shown in Figure 4 are calculated as follows:

$$\begin{cases} A_d = a \cdot c \\ A_c = e \cdot (a \cdot b) \end{cases} \tag{9}$$

The above calculation results are shown in Table 2.

**Table 2.** Structure parameters of C-type Fe-based nanocrystalline iron core.

Item	Unit	Value	Item	Unit	Value
<i>a</i>	mm	141	<i>e</i>	mm	25
<i>b</i>	mm	190	<i>f</i>	mm	25
<i>c</i>	mm	40.5	$A_c$	cm <sup>2</sup>	6
<i>d</i>	mm	90	$A_d$	cm <sup>2</sup>	57.1

3.3. DC Bias Model

A series DC voltage source is used to simulate the intrusion of DC components. The circuit diagram is shown in Figure 7. The effects of different DC components on the electromagnetic vibration characteristics of HFT with different windings are studied, respectively. The DC bias coefficient  $H_{dc}$  of HFT is defined as the ratio of DC voltage peak value to AC voltage peak value:  $H_{dc} = 100 U_{dc}/U_{ac}$ . The effective value of AC voltage source is kept unchanged, and different DC bias coefficients  $H_{dc}$  are selected as 0, 0.2, 0.4 and 0.6 for excitation current experiment.

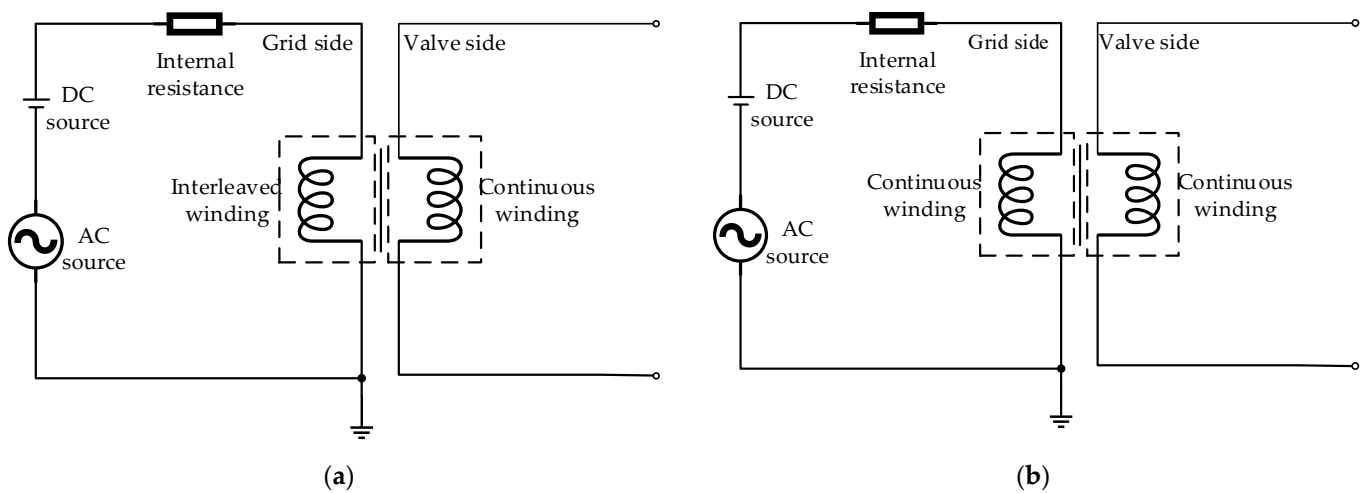


**Figure 7.** Coupling circuit structure under DC bias. (a) Interleaved windings; (b) Continuous windings.

In the multi-physics field calculation of HFT, the FEM adopts sequential coupling method to calculate the vibration of HFT. The multi-physics field coupling simulation process is shown in Figure 8.

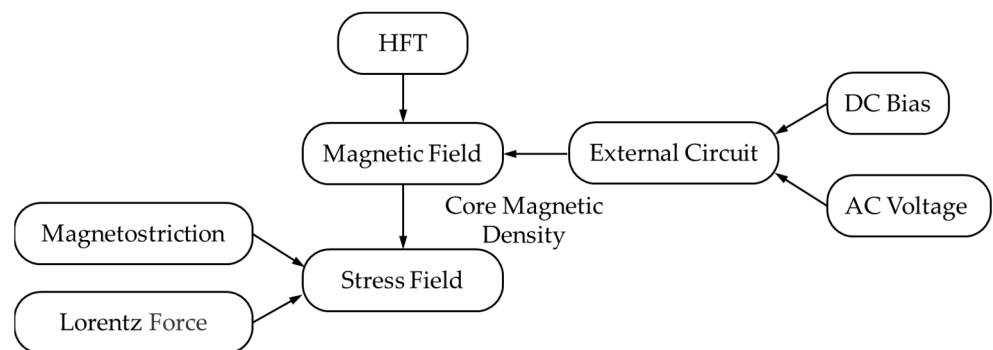


**Figure 8.** Multi-physics field coupling calculation flow chart of HFT.

#### 4. Analysis of Electromagnetic Vibration Characteristics under DC Bias

##### 4.1. Electromagnetic Characteristics

Since HFT has a high operating frequency and large coil reactance, its current waveform is unstable at the initial moment, resulting in local oscillation. The excitation current in continuous winding tends to be stable at 0.0348 s. However, the interleaved winding can suppress the oscillation caused by external impact, so its current stabilization time is shorter at 0.012 s. The current waveform is strictly symmetric about the timeline. Figure 9 shows the time-domain waveform of excitation current under different DC bias coefficients  $H_{dc}$ .

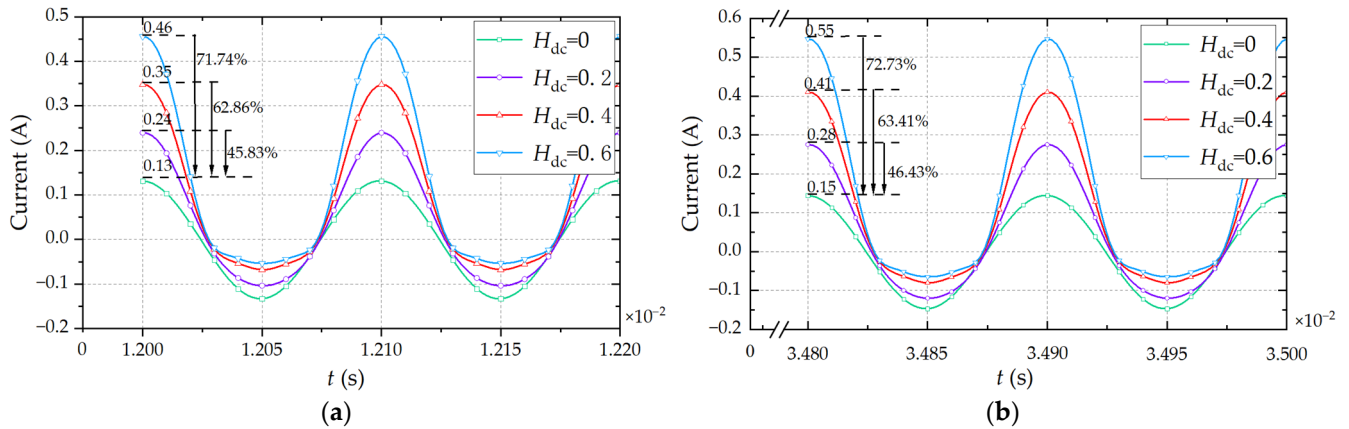


**Figure 9.** Schematic diagram of excitation current under different DC bias coefficients. (a) Interleaved windings; (b) Continuous windings.

Both HFT models mentioned above are excited by voltage source. The excitation current is obtained by simulation. Interleaved windings are wound together with two wires, and then the taps are welded. Compared with continuous winding, the inter-turn connection of interleaved winding is more complicated. Interleaved winding adopts wire transposition. Therefore, the copper consumption of winding is more than that of continuous winding. Under the no-load condition without DC bias, the excitation current is slightly smaller. With the increase in DC bias component, the positive peak value of excitation current increases gradually, and the negative peak value decreases gradually. When the DC bias coefficient  $H_{dc}$  increases to 0.6, the positive peak value of the continuous winding excitation current is 0.55 A, about four times of the peak value of rated no-load current. In addition, the positive peak value of the interleaved winding excitation current is 0.46 A, about 3.5 times that of the peak value of rated no-load current. It is slightly less than the growth ratio of continuous winding, and the same rule is also true under other DC bias coefficients. It can be seen that the interleaved winding can suppress the increase in current more than continuous winding, thereby suppressing saturation of the iron core. However, with the increase in applied voltage, both have different degrees of “positive half-cycle saturation and negative half-cycle attenuation”. It is mainly caused by the nonlinear magnetic characteristics of iron core.

Fourier transform is performed on the excitation current test results under different DC bias coefficients to obtain the excitation current spectrum as shown in Figure 10. When there is no DC supply, the excitation current is mainly odd harmonics, and even harmonics content is very small. With the increase in DC voltage, the harmonics in excitation current increase continuously. This is because when the DC magnetic flux in the iron core continues to increase, the positive half wave increases sharply, and the negative half wave decreases slowly. The saturation of the iron core increases, resulting in more and more serious distortion. It can be seen that DC bias increases the harmonic components of each frequency in the excitation current, and the excitation current shows a spike wave.

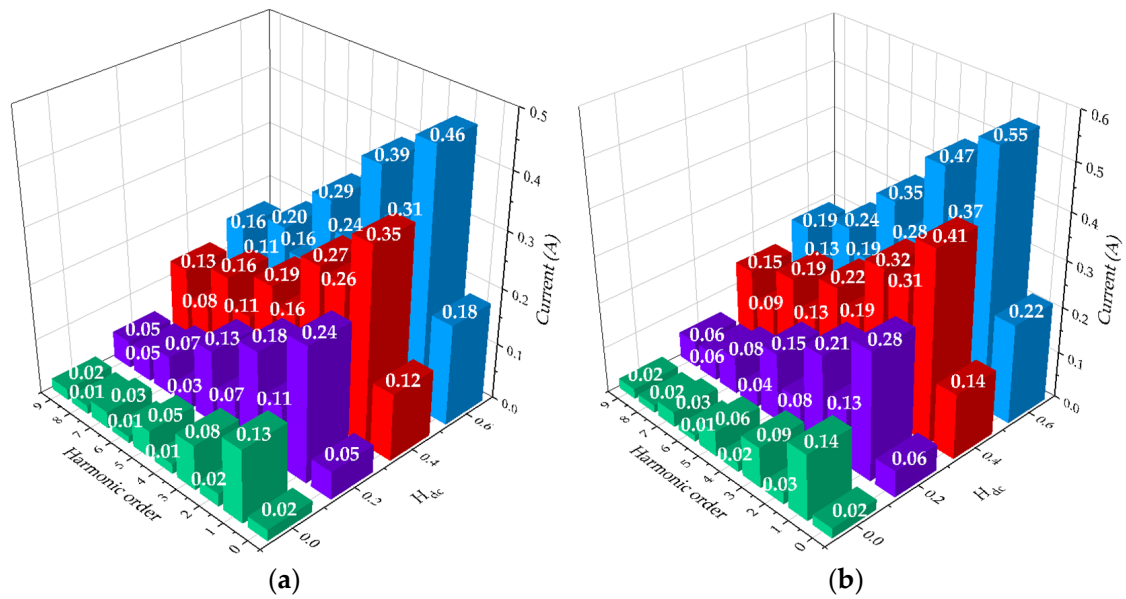


Figure 10. Excitation current spectrum analysis. (a) Interleaved windings; (b) Continuous windings.

Figure 11 shows the magnetic flux density distribution of iron core under a different DC component. When the DC current increases to saturation, the DC magnetic flux density increases gradually. Compared with continuous winding, the interleaved winding has advantages of suppressing applied voltage, which makes the core magnetic density increase more slowly. Before the DC component is added, the magnetic flux is mainly distributed in iron core limb. The magnetic flux density of the upper and lower yokes is not consistent. With the increase in DC component, the distribution of magnetic flux density becomes disordered, and the magnetic flux density is distributed in each position of the iron core. This is because the corresponding change in magnetic flux of HFT is sinusoidal without DC bias. When the DC bias occurs, the magnetic flux density curve is no longer symmetrical with time, and the length of its positive and negative half waves is different, resulting in different equivalent frequencies.

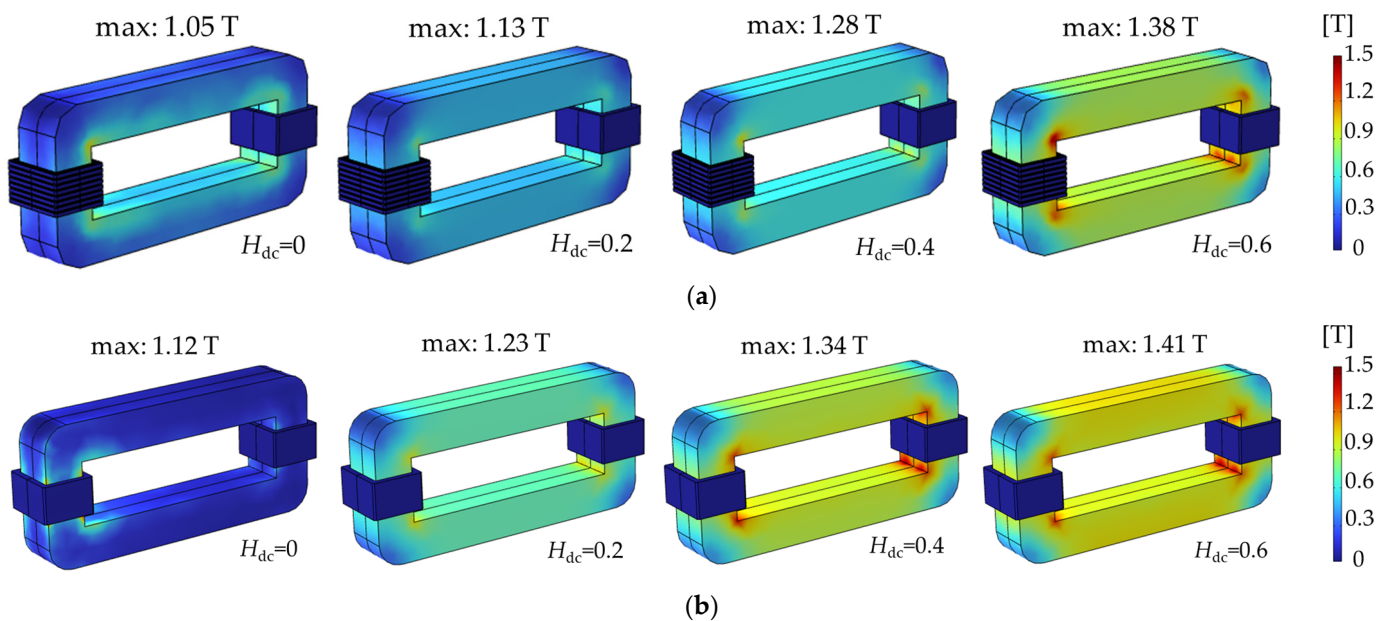


Figure 11. Magnetic flux density distribution. (a) Interleaved windings; (b) Continuous windings.

Table 3 summarizes the electromagnetic characteristic parameters including loss density of iron core and windings of HFT at a different DC component. For the HFT with continuous winding, as the DC bias coefficient increases from 0 to 0.6, the iron loss increases from  $3.58 \times 10^6 \text{ W/m}^3$  to  $8.69 \times 10^6 \text{ W/m}^3$ . In particular, when the DC bias coefficient increases from 0.2 to 0.6, the iron loss density increases dramatically. This is because the positive half wave peak value of magnetic flux density curve increases continuously under the effect of DC bias. The iron core gradually reaches saturation, and the operating point of iron core constantly approaches the saturation area of hysteresis loop, which makes the leakage flux and loss of HFT rise sharply. When the DC bias coefficient increases from 0 to 0.6, the loss density of windings increases from  $1.40 \times 10^6 \text{ W/m}^3$  to  $2.19 \times 10^6 \text{ W/m}^3$ . On the one hand, this is because the heating caused by the increase in excitation current. On the other hand, because the iron core is saturated, more excitation power is required. The same is true for HFT with interleaved winding, but its loss is smaller than that of HFT with continuous winding.

**Table 3.** Electromagnetic parameters with different DC bias.

Winding Type	$H_{dc}$	Maximum Magnetic Flux Density (T)	Average Core Loss Density ( $\text{W/m}^3$ )	Average Winding Loss Density ( $\text{W/m}^3$ )
Interleaved winding	0	1.05	$3.43 \times 10^6$	$1.12 \times 10^6$
	0.2	1.13	$4.25 \times 10^6$	$1.54 \times 10^6$
	0.4	1.28	$5.80 \times 10^6$	$1.86 \times 10^6$
	0.6	1.38	$8.39 \times 10^6$	$1.91 \times 10^6$
Continuous winding	0	1.12	$3.58 \times 10^6$	$1.40 \times 10^6$
	0.2	1.23	$4.39 \times 10^6$	$1.91 \times 10^6$
	0.4	1.34	$6.16 \times 10^6$	$2.11 \times 10^6$
	0.6	1.41	$8.69 \times 10^6$	$2.19 \times 10^6$

#### 4.2. Vibration Characteristics

Table 4 summarizes the vibration characteristic parameters of HFT at different DC bias component. It can be seen that there are two different stress and deformation distribution patterns before and after increasing the DC component. The stress points become more and more disordered under the influence of DC component. For the HFT with continuous winding, the maximum stress on iron core increases from  $9.21 \times 10^5 \text{ N/m}^2$  to  $3.94 \times 10^6 \text{ N/m}^2$  with the increase in DC component. In addition, the maximum stress on windings increases from  $5.31 \times 10^5 \text{ N/m}^2$  to  $1.82 \times 10^6 \text{ N/m}^2$ , which is determined by the current flowing through windings. The distribution of Lorentz force in windings becomes wider and wider. Similarly, the HFT with interleaved winding also has the distribution patterns mentioned above, but the stress is reduced in different degrees.

**Table 4.** Vibration parameters with different DC bias.

Winding Type	$H_{dc}$	Maximum Iron Core Stress ( $\text{N/m}^2$ )	Maximum Winding Stress ( $\text{N/m}^2$ )	Maximum Iron Core Deformation (m)	Maximum Winding Deformation (m)
Interleaved winding	0	$8.91 \times 10^5$	$4.96 \times 10^5$	$4.28 \times 10^{-6}$	$1.01 \times 10^{-6}$
	0.2	$1.86 \times 10^6$	$8.49 \times 10^5$	$6.79 \times 10^{-6}$	$2.96 \times 10^{-6}$
	0.4	$3.39 \times 10^6$	$1.53 \times 10^6$	$9.97 \times 10^{-6}$	$6.29 \times 10^{-6}$
	0.6	$4.03 \times 10^6$	$1.78 \times 10^6$	$1.07 \times 10^{-5}$	$7.99 \times 10^{-6}$
Continuous winding	0	$9.21 \times 10^5$	$5.31 \times 10^5$	$4.39 \times 10^{-6}$	$1.03 \times 10^{-6}$
	0.2	$1.97 \times 10^6$	$8.64 \times 10^5$	$6.97 \times 10^{-6}$	$3.29 \times 10^{-6}$
	0.4	$3.56 \times 10^6$	$1.63 \times 10^6$	$1.03 \times 10^{-5}$	$7.36 \times 10^{-6}$
	0.6	$3.94 \times 10^6$	$1.82 \times 10^6$	$1.18 \times 10^{-5}$	$8.22 \times 10^{-6}$

Figure 12 shows the overall deformation of HFT with interleaved winding. Figures 13 and 14 show the deformation characteristics of iron core and winding under

a different DC component. The deformation law corresponds to the stress distribution, that is, the deformation increases with the increase in DC component. For the HFT with continuous winding, the maximum vibration displacement of iron core without DC bias is  $4.39 \times 10^{-6}$  m. When  $H_{dc}$  increases to 0.6, the maximum vibration displacement reaches  $1.18 \times 10^{-5}$  m, about 2.7 times that of the peak value of displacement without DC bias. It can be seen from the winding deformation characteristic diagram that the maximum vibration displacement of windings without DC bias is  $1.03 \times 10^{-6}$  m. When  $H_{dc}$  increases to 0.6, the maximum vibration displacement is  $8.22 \times 10^{-6}$  m, about 8.0 times that of the peak value of displacement without DC bias. For the HFT with interleaved winding, the core magnetic density and excitation current are smaller than those of the HFT with continuous winding at the same DC bias level, so the displacement of core and winding is smaller.

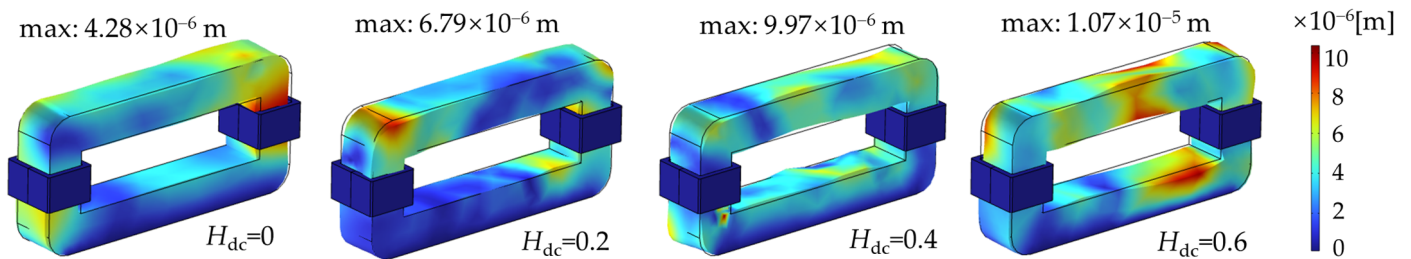


Figure 12. Overall deformation distribution of HFT with interleaved winding.

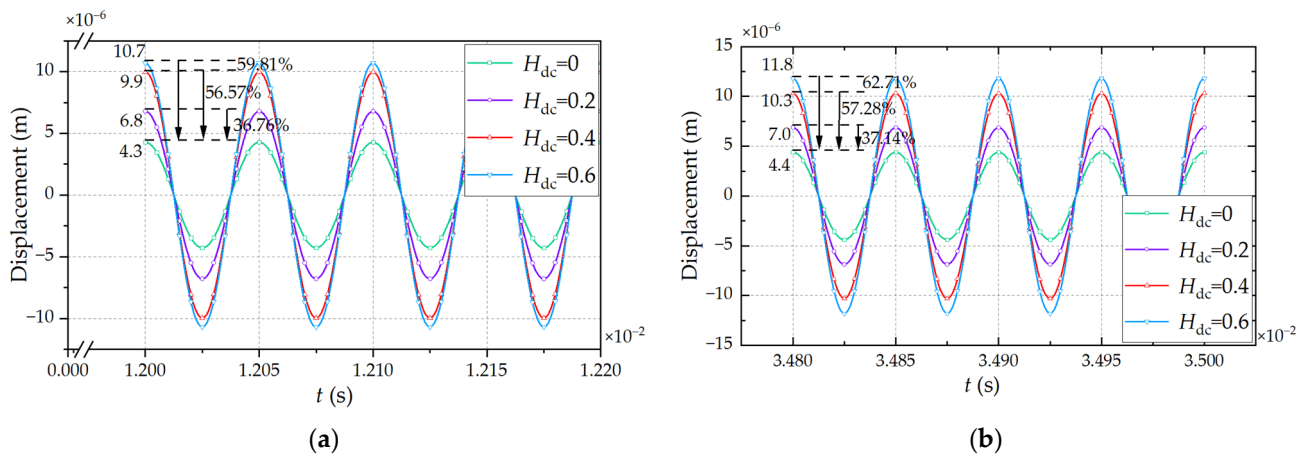


Figure 13. Iron core deformation characteristics. (a) Interleaved windings; (b) Continuous windings.

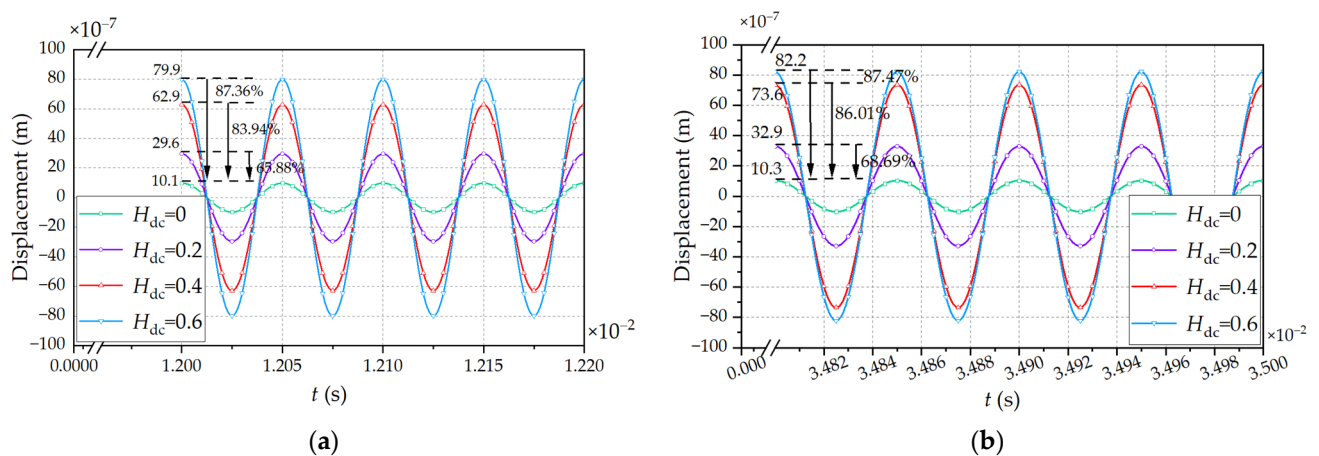


Figure 14. Winding deformation characteristics. (a) Interleaved windings; (b) Continuous windings.

## 5. Conclusions

In this paper, the characteristics of HFT with different winding structures are compared by establishing a multi-physical coupling model of 500 V HFT under DC bias. The electromagnetic field and stress field of transformer under no load are simulated, and the short-circuit current, loss, magnetic flux density, vibration stress and displacement of HFT with different windings are obtained. The electromagnetic vibration law of iron core and winding is effectively simulated. The following conclusions are drawn:

With the increase in the DC bias coefficient, the excitation current amplitude of positive half cycle increases, the amplitude of negative half cycle decreases, and the harmonic components of each excitation current frequency gradually increase. The distribution of main magnetic flux density is gradually distorted, and its amplitude increases gradually. When the DC bias coefficient increases to the core magnetic density saturation, the increase in magnetic flux density is no longer obvious. The core loss increases sharply. On the contrary, the winding loss increases slowly.

The stress and displacement of iron core and winding increase with the increase in DC component, but the increasing amplitude of the stress and displacement of iron core decreases after saturation. Under the same DC bias level, the current fluctuation and vibration in interleaved winding are smaller, which proves that the interleaved winding is more capable of resisting external impulse voltage than the continuous winding.

**Author Contributions:** Conceptualization, W.Z. and H.D.; methodology, W.Z. and H.D.; software, H.D. and Y.S.; validation, H.D., W.Z. and Y.S.; formal analysis, H.D.; investigation, W.Z.; resources, Y.S.; data curation, H.D. and Y.S.; writing—original draft preparation, H.D. and Y.S.; writing—review and editing, W.Z., M.L. and L.Z.; visualization, W.Z., M.L. and L.Z.; supervision, W.Z., M.L. and L.Z.; project administration, W.Z., M.L. and L.Z.; funding acquisition, W.Z., M.L. and L.Z. All authors have read and agreed to the published version of the manuscript.

**Funding:** This research was funded by the Project of National Key Research and Development Program of China, grant number 2022YFB2404100.

**Data Availability Statement:** The original data supporting the conclusion of this paper can be directly provided by the authors.

**Conflicts of Interest:** The authors declare no conflict of interest.

## References

1. Chen, Z.; Li, H.; Liu, L.; Xiang, L.; Bai, B. DC Bias Treatment of Hybrid Type Transformer Based on Magnetic Flux Modulation Mechanism. *IEEE Trans. Magn.* **2019**, *55*, 1700204. [[CrossRef](#)]
2. Pan, C.; Wang, C.J.; Su, H. Excitation Current and Vibration Characteristics of DC Biased Transformer. *CSEE J. Power Energy Syst.* **2021**, *7*, 604–613.
3. Li, X.; Wen, X.; Markham, P.N.; Liu, Y. Analysis of Nonlinear Characteristics for a Three-Phase, Five-Limb Transformer under DC Bias. *IEEE Trans. Power Deliv.* **2010**, *25*, 2504–2510. [[CrossRef](#)]
4. Yang, C.; Ding, Y.; Qiu, H.; Xiong, B. Analysis of Turn-to-Turn Fault on Split-Winding Transformer Using Coupled Field-Circuit Approach. *Processes* **2021**, *9*, 1314. [[CrossRef](#)]
5. Zhang, X.; Liu, X.; Guo, F. Calculation of DC Bias Reactive Power Loss of Converter Transformer via Finite Element Analysis. *IEEE Trans. Power Deliv.* **2020**, *36*, 751–759. [[CrossRef](#)]
6. Liu, C.M.; Li, X.H.; Li, X.J. Simulating the Vibration Increase of the Transformer Iron Core due to the DC Bias. *Int. J. Appl. Electron. Mech.* **2017**, *55*, 423–433. [[CrossRef](#)]
7. Biró, O.; Koczka, G.; Leber, G.; Preis, K.; Wagner, B. Finite Element Analysis of Three-Phase Three-Limb Power Transformers under DC Bias. *IEEE Trans. Magn.* **2014**, *50*, 565–568. [[CrossRef](#)]
8. Fuchs, E.F.; You, Y.; Roesler, D.J. Modeling and Simulation, and Their Validation of Three-Phase Transformers with Three Legs under DC Bias. *IEEE Trans. Power Deliv.* **1999**, *14*, 443–449. [[CrossRef](#)]
9. Zhao, Z.G.; Liu, F.G.; Cheng, Z.G.; Yan, W.L.; Liu, L.R.; Zhang, J.J.; Fan, Y.N. Measurements and Calculation of Core-Based  $B-H$  Curve and Magnetizing Current in DC-Biased Transformers. *IEEE Trans. Appl. Supercond.* **2010**, *20*, 1131–1134. [[CrossRef](#)]
10. Chen, D.; Feng, Z.; Wang, Q.; Fang, L.; Bai, B. Study of Analysis and Experiment for Ability to Withstand DC Bias in Power Transformers. *IEEE Trans. Magn.* **2018**, *54*, 1–6. [[CrossRef](#)]
11. Chen, Y.; Fu, W.; Lin, H.; Niu, S. A Passive Negative Magnetic Reluctance Structure-Based kHz Transformer for Improved DC Magnetic Bias Withstanding. *IEEE Trans. Power Electron.* **2023**, *38*, 717–727. [[CrossRef](#)]

12. Zhou, Z.Q.; Duan, H.; Cheng, L.; Xie, Q.; Chen, D.Z. Study on Influence of Different Winding Structure Parameters on Insulation Structure of UHV Converter Transformer. *Transformer* **2022**, *59*, 36–42.
13. Zhang, J.H. Control Measures of Creepage between Transformer Disc Coils. *Transformer* **2019**, *56*, 18–20.
14. Luo, Q.L.; Luo, Q.S.; Wang, B. Research and Calculation of Longitudinal Insulation in Special Interleaved Winding of Converter Transformer. *Transformer* **2013**, *50*, 1–4.
15. Zhang, B.; Zhang, Q. Characteristic Analysis of Magnetic Resonant Coupling-Based Wireless Power Transfer System with Two Receivers. *J. South Chin. Univ. Technol.* **2012**, *40*, 152–158.
16. Sawahara, Y.; Futagami, D.; Ishizaki, T.; Awai, I. Development of underwater WPT system independent of salinity. In Proceedings of the 2014 Asia-Pacific Microwave Conference (APMC), Sendai, Japan, 4–7 November 2014; pp. 1363–1365.
17. Li, J.; Zhang, P.; Ma, T.; Zhang, Y.; Wang, Y.W.; Wei, C.; Wang, B. Simulation and experimental analysis of wireless power transmission system via magnetic resonance coupling. *Electr. Mach. Control* **2015**, *19*, 72–78.
18. Yang, Y.M.; Liu, X.M.; Yang, F.; Jadoon, A.; Zhang, C.Y. Analysis of DC bias vibration of transformer core based on electromagnetic force field coupling. *Int. J. Appl. Electrom. Mech.* **2014**, *50*, 297–309. [[CrossRef](#)]
19. Georgi, S.; Helmut, P.; Peter, H. Spatial Distributions of Magnetostriction Displacements and Noise Generation of Model Transformer Cores. *Int. J. Mech. Sci.* **2016**, *118*, 188–194.
20. Pfutzner, H.; Shilyashki, G.; Bengtsson, C. Effects of DC Bias on Regional Flux and Magnetostriction of A Single-Phase Transformer Core Modeled by 3-D MACC. *IEEE Trans. Magn.* **2018**, *54*, 1–6. [[CrossRef](#)]
21. Li, B.; Wang, Z.Z. Research on Winding Current of UHV Transformer under DC-Bias. *Trans. Chin. Electrotech. Soc.* **2020**, *35*, 1422–1431.
22. Liu, T.; Wu, H.; Liu, L.; Peng, Z.; Wang, H. Simulation of Losses in DC-Biased Single Phase Three Limb Transformer. In Proceedings of the 2016 IEEE International Conference on High Voltage Engineering and Application (ICHVE), Chongqing, China, 19–22 September 2016; pp. 1–4.
23. Pan, Z.H.; Wang, X.M.; Tan, B.; Zhu, L.; Liu, Y.; Liu, Y.L.; Wen, X.S. Potential Compensation Method for Restraining the DC Bias of Transformers During HVDC Monopolar Operation. *IEEE Trans. Power Deliv.* **2016**, *31*, 103–111. [[CrossRef](#)]
24. Yang, Y.M.; Liu, X.M.; Yang, F. Soil structure effect on transformer DC bias. In Proceedings of the 2014 IEEE International Conference on Industrial Technology (ICIT), Busan, Republic of Korea, 26 February–1 March 2014; pp. 535–540.

**Disclaimer/Publisher’s Note:** The statements, opinions and data contained in all publications are solely those of the individual author(s) and contributor(s) and not of MDPI and/or the editor(s). MDPI and/or the editor(s) disclaim responsibility for any injury to people or property resulting from any ideas, methods, instructions or products referred to in the content.